Inhibition of the MYC-Regulated Glutaminase Metabolic Axis Is an Effective Synthetic Lethal Approach for Treating Chemoresistant Ovarian Cancers

Yao-An Shen[1,2,3], Jiaxin Hong[1,2], Ryoichi Asaka[1,2], Shiho Asaka[1], Fang-Chi Hsu[1,4], Yohan Suryo Rahmanto[1,2], Jin-Gyoung Jung[1,2], Yu-Wei Chen[1,3], Ting-Tai Yen[1,3], Alicja Tomaszewski[1,3], Cissy Zhang[2], Nabeel Attarwala[2], Angelo M. DeMarzo[1,2], Ben Davidson[5], Chi-Mu Chuang[6,7], Xi Chen[8], Stephanie Gaillard[1,3], Anne Le[2], Ie-Ming Shih[1,2,3], and Tian-Li Wang[1,2,3]

ABSTRACT

Amplification and overexpression of the *MYC* oncogene in tumor cells, including ovarian cancer cells, correlates with poor responses to chemotherapy. As MYC is not directly targetable, we have analyzed molecular pathways downstream of MYC to identify potential therapeutic targets. Here we report that ovarian cancer cells overexpressing glutaminase (GLS), a target of MYC and a key enzyme in glutaminolysis, are intrinsically resistant to platinum-based chemotherapy and are enriched with intracellular antioxidant glutathione. Deprivation of glutamine by glutamine-withdrawal, GLS knockdown, or exposure to the GLS inhibitor CB-839 resulted in robust induction of reactive oxygen species in high GLS-expressing but not in low GLS-expressing ovarian cancer cells. Treatment with CB-839 rendered GLS^{high} cells vulnerable to the poly(ADP-ribose) polymerase (PARP) inhibitor, olaparib, and prolonged survival in tumor-bearing mice. These findings suggest consideration of applying a combined therapy of GLS inhibitor and PARP inhibitor to treat chemoresistant ovarian cancers, especially those with high GLS expression.

Significance: Targeting glutaminase disturbs redox homeostasis and nucleotide synthesis and causes replication stress in cancer cells, representing an exploitable vulnerability for the development of effective therapeutics.

Graphical Abstract: http://cancerres.aacrjournals.org/content/canres/80/20/4514/F1.large.jpg.

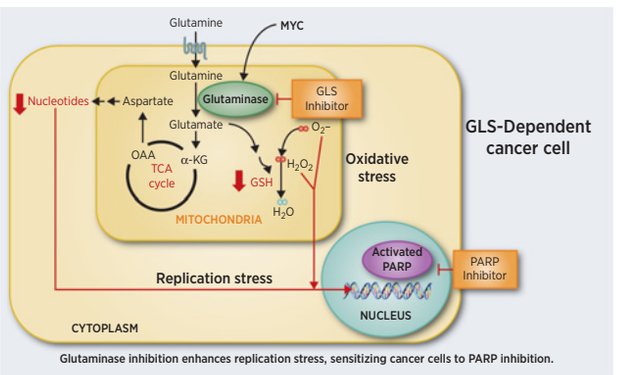

Glutaminase inhibition enhances replication stress, sensitizing cancer cells to PARP inhibition.

Introduction

Ovarian cancer is a highly aggressive disease, and patients are often refractory to the frontline chemotherapy (carboplatin and paclitaxel) or develop drug resistance after multiple rounds of chemotherapy (1). Developing new therapeutics to enhance treatment response and to eradicate drug-resistant ovarian cancers have become an unmet need for improving patient prognosis. Accumulating evidence suggests that *MYC* oncogene amplification and/or overexpression plays an important role in the pathogenesis of a significant fraction of ovarian cancers (2). The MYC protein can upregulate glutamine metabolism, and *MYC*-transformed cells rely predominantly on exogenous glutamine for survival and growth (3). Although MYC protein is considered not directly targetable, inhibitors that inactivate key enzymes of the glutamine pathway are available, and hold promise as new cancer therapeutic agents.

Glutamine (GLN) is the most abundant nonessential amino acid in the bloodstream and in the rapidly dividing cells such as cancer cells. Glutamine serves as a precursor for replenishing tricarboxylic (TCA) cycle intermediates for generating ATP and for biosynthesis of key macromolecules for nucleotide synthesis (4). Many cancer cells use glutamine as a major carbon source to fuel TCA cycle–dependent anabolic growth via oxidative or reductive carboxylation (5). Cancer

[1]Sidney Kimmel Comprehensive Cancer Center, Johns Hopkins University School of Medicine, Baltimore, Maryland. [2]Department of Pathology, Johns Hopkins University School of Medicine, Baltimore, Maryland. [3]Department of Gynecology and Obstetrics, Johns Hopkins University School of Medicine, Baltimore, Maryland. [4]The Ph.D. Program for Translational Medicine, College of Medical Science and Technology, Taipei Medical University and Academia Sinica, Taipei, Taiwan. [5]Department of Pathology, Norwegian Radium Hospital, Oslo University Hospital, and Institute of Clinical Medicine, Faculty of Medicine, University of Oslo, Oslo, Norway. [6]College of Nursing, National Taipei University of Nursing and Health Sciences, Taipei, Taiwan. [7]Department of Obstetrics and Gynecology, Taipei Veterans General Hospital, Taipei, Taiwan. [8]Bradley Department of Electrical and Computer Engineering, Virginia Tech, Arlington, Virginia.

Note: Supplementary data for this article are available at Cancer Research Online (http://cancerres.aacrjournals.org/).

Corresponding Authors: Tian-Li Wang, Johns Hopkins University School of Medicine, Room 306, CRB2, 1550 Orleans Street, Baltimore, MD 21231. Phone: 410-502-0863; E-mail: tlw@jhmi.edu; and Ie-Ming Shih, Johns Hopkins Medical Institutions, Room 305, CRB2, 1550 Orleans Street, Baltimore, MD 21231. Phone: 410-502-7774; E-mail: ishih@jhmi.edu

Cancer Res 2020;80:4514–26

doi: 10.1158/0008-5472.CAN-19-3971

cells may also shunt glutamine-derived metabolic intermediates to the production of glutathione (GSH) and NAD(P)H for cellular redox homeostasis (6). Glutamine input is the rate-limiting step in glutathione synthesis (7) and can neutralize peroxide-free radicals through the production of NADPH via mitochondrial enzymes such as malic enzyme, isocitrate dehydrogenase (IDH), and glutamate dehydrogenase (8–10). Deprivation of glutamine or administration of the glutaminase (GLS) inhibitor, BPTES, has been reported to stimulate ROS production, induce endoplasmic reticulum stress, and suppress oxidative phosphorylation in mitochondria (11, 12). As the level of reduced GSH is tightly correlated with tumorigenesis and therapeutic resistance in cancer (13), inhibiting glutamine metabolism is considered a promising therapeutic strategy to overcome clinical resistance.

The current study indicates that MYC may directly regulate key enzymes in the glutaminolysis pathway including mitochondrial GLS, which is upstream of the glutaminolysis pathway and catalyzes conversion of glutamine to glutamate (5). Downstream of GLS are RRM2 and SHMT2, also MYC targets, and they catalyze *de novo* nucleotide synthesis and glutathione synthesis, respectively. Pharmacological inhibitors of these enzymes have been developed and some of them have demonstrated promising antitumor efficacy (5). Because GLS is pivotal in the glutaminolysis pathway and specific pharmacologic inhibitors of GLS such as CB-839 are currently being evaluated in phase II clinical trials, the current study focuses on understanding the mechanisms by which GLS inhibition suppresses GLS^{high} ovarian cancer cells. The results provide a biological rationale for exploring another cancer drug that could act synergistically with GLS inhibitors to overcome or delay resistance to cancer treatment.

Following this strategy, GLS inhibitors have been shown to act synergistically with several anticancer drugs including erlotinib (an EGF tyrosine kinase receptor inhibitor) for EGFR-mutant lung cancer (14), β-lapachone (a natural o-naphthoquinone compound) for pancreatic cancer (15), 5-azacitidine or BCL2 inhibition for acute myeloid leukemia (16, 17), and HSP90 inhibitor for mTORC1-driven tumor cells (18). In ovarian cancer, platinum-resistant tumor cells show an increase in glutamine metabolism and GLS inhibitors, BPTES and 968, sensitize chemoresistant ovarian cancer cells to platinum-based chemotherapeutic drugs (19–21). However, these studies were performed on cell culture models, were restricted to the use of nonclinical-grade inhibitors, and involved drug interactions (e.g., BPTES and platinum) whose combinatorial mechanisms are unclear. In addition to discovering a MYC regulatory link, the current study fills in these knowledge gaps and provides critical data applicable to the development of future translational applications. Our results demonstrate that inactivating GLS compromises redox homeostasis, suppresses nucleotide synthesis, and causes replication stress. GLS inhibitor treatment renders cancer cells dependent on PARP DNA repair and sensitizes ovarian cancer to the PARP inhibitors.

Materials and Methods

Reagents and cell lines

Small-molecule inhibitors were purchased from the following vendors: olaparib (cat no. S1060, Selleckchem), N-acetyl-L-cysteine (cat no. A7250 Sigma-Aldrich), and dimethyl 2-oxoglutarate (cat no. 349631 Sigma-Aldrich). CB-839 was kindly provided by Calithera Biosciences. Drug dilution, use, and storage were performed following standard protocols. The final concentration of DMSO for *in vitro* cell biology experiments was maintained at levels ≤0.1%.

Cyst108, FT105, FT2821, and FT406 were primary cultures, and were grown in DMEM with 15% FBS. The other cell lines were cultured in RPMI-1640 with 10% FBS. For glutamine deprivation, cells were cultured in glutamine-free and pyruvate-free DMEM with 4.5 g/L glucose (Fisher Scientific; cat no. SH30081) and 10% dialyzed FBS (Invitrogen; cat no. 26400). For glucose deprivation, cells were cultured in glucose-free DMEM (Invitrogen; cat no: A14430) with 10% FBS.

Cell line source

IOSE-80PC (22) and MPSC1 (23) were described previously. Ovarian surface epithelial cells (OSE10) were a kind gift from Dr. H Katabuchi, Kumamoto University, Japan (24). Between 2001 and 2012, KOV3, OVCAR3, OVCAR5, OVCAR8, TOV-21G, ES-2, TOV-112D, and Hey were obtained from the ATCC; OAW28 was obtained from the European Collection of Authenticated Cell Cultures (ECACC). OVCAR5 was initially reported as an epithelial ovarian cancer cell line; however, results from a recent study suggest that OVCAR5 may have originated from a gastrointestinal tumor (25). Ovarian clear cell carcinoma cell lines, OVISE, OVMANA, and OVTOKO, were obtained from the Japanese Collection of Research Bioresources, and JHOC-5 from the RIKEN. They were obtained between 2010 and 2014.

Cell line authentication

The short tandem repeat (STR) profiles of SKOV3, OVCAR5, OVISE, and IOSE-80PC were verified in our previously studies (4–6). The STR profiles of OV429 and OVCAR8 were analyzed in September 2019. STR analysis was performed by the Fragment Analysis Facility at Johns Hopkins University using the STR DNA profiling primers from Promega (PowerPlex 1.2 System, Promega). STR profiles were compared with the profiles in the Cellosaurus STR Database. *Mycoplasma* status of the cell lines were tested routinely using a kit purchased from the ATCC; the most recent test dated in May 2020.

Chromatin immunoprecipitation sequencing analysis and data deposition

Chromatin immunoprecipitation sequencing (ChIP-seq) FATSQ data were processed by Bowtie 2 and aligned to hg19 reference index (26). ChIP-seq peak calling was performed by MACS2 and ChIP-seq peaks were visualized by Integrative Genomics Viewer (27). Peak annotation, gene symbol conversion, and *q*-values were performed by R packages. ChIP-seq FASTQ files have been deposited at the Gene-Expression Omnibus under accession number GSE154941.

Tissue specimens

Formalin-fixed and paraffin-embedded primary ovarian cancer tissues were obtained from the Department of Pathology at the Johns Hopkins Hospital, Baltimore, Maryland. Specimens with tumor cell population > 50% and minimal or no necrosis were included in this study. Specimens were arranged in tissue microarrays to facilitate IHC and to ensure that the tissues were stained under the same conditions. The Norwegian cohort consisted of ascites tumors from 195 patients who had previously received platinum-based chemotherapy. The study was approved by the Johns Hopkins University School of Medicine Institutional Review Board and the Regional Committee for Medical Research Ethics in Norway (S-04300).

Experimental animals and metabolite analysis in tissue samples

All mice used in *in vivo* experiments including those involving xenograft mice were maintained and handled according to the specified approved protocol and guidelines issued by the Johns Hopkins University Animal Care and Use Committee. To test *in vivo* drug

efficacy, 2×10^6 ES-2 or OV2008 cells were injected into the subcutaneous region of athymic *nu/nu* mice. Once tumors reached an average volume of 100 mm^3, mice were randomized into 4 arms and treated with vehicle DMSO (1%), olaparib (75 mg/kg, intraperitoneal injection, once daily), CB-839 (200 mg/kg, oral gavage, twice daily), or a combination of olaparib and CB-839. Tumor dimensions were measured by a Vernier caliper every other day. Tumor volume was calculated using the following formula: $0.5 \times \text{length} \times (\text{width})^2$.

Tumors were snap frozen in liquid N_2 for later metabolite extraction and analysis. Tumors were initially homogenized in 80%/20% methanol/water, and centrifuged at $14{,}000 \times g$ for 10 minutes. The resulting supernatant was transferred to a new tube. Another round of extraction was performed on the pellet by suspending it in 80/20% methanol/water, followed by centrifugation at $14{,}000 \times g$ for 10 minutes. Supernatant samples were dried at room temperature for 60 minutes using a Speed Vac system, lyophilized, and stored at −80°C for LC/MS analysis. An Agilent 6545 Quadrupole–Time-of-Flight (Q-TOF) mass spectrometer with an Agilent 1260 HPLC at the Metabolomics Core Facility at the Johns Hopkins Medical Institutions was used for acquiring metabolomics data from samples. An HPLC-autosampler system was used to take up 2 μL into the system. All procedures were performed at 4°C to provide a stable environment. A Discovery HS F5 HPLC Column (Sigma) was used at a flow rate of 0.15 mL/min. Spectra were mass calibrated throughout data acquisition against a reference calibrant. Metabolites were identified using our own compound standard databases of identified retention times, and MS/MS fragmentation data were used to confirm the identity of metabolites. Additional analysis using an Agilent 6490 triple-quadrupole (QQQ) mass spectrometer was performed to confirm the findings from discovery and qualitative screening experiments using Q-TOF mass spectrometry. To determine the metabolic composition of every sample, we used Agilent MassHunter, Agilent Mass Profiler Professional, and Agilent Qualitative and Quantitative Analysis Software packages. Metabolite peak intensities were normalized to the protein concentration.

Statistical analysis

GraphPad Prism 7 was used for statistical analysis and graph generation. Multiple tests were utilized to assess statistical significance and indicated in figure legends. All data are presented as mean ± SEM, and differences between groups with $P \leq 0.05$ were considered statistically significant. For data presented in **Fig. 3C**, patients were separated into GLS^{high} ($n = 99$) and GLS^{low} ($n = 96$) groups. Overall survival was analyzed by Kaplan–Meier curve and log-rank test using SPSS version 25.

Results

MYC activates transcription of genes in multiple functional pathways including glutamine metabolism

MYC plays a pivotal role in tumorigenesis through transcriptional regulation of genes involved in metabolism, macromolecule biosynthesis, and cell-cycle progression. Overexpression or amplification of MYC causes dysregulated transcription of target genes that contribute to cancer-associated phenotypes. Because MYC may regulate transcription under specific conditions for specific cell types, the identities of MYC target genes in ovarian cancer remain uncertain, despite the fact that MYC is amplified and overexpressed in more than 30% of human ovarian cancers. We therefore performed chromatin immunoprecipitation sequencing (ChIP-seq) on OVCAR3 cells in which MYC was amplified to identify MYC target genes. We also performed MYC ChIP-seq on MCF7 cells, which overexpress MYC. In total, 4,868 MYC ChIP-seq peaks were identified in OVCAR3 cells and 5,979 in MCF7 cells (MACS2, q-value < 0.01). Motif enrichment analysis was performed on MYC ChIPed DNA sequences using the HOMER software package (28), and the well-characterized MYC E-box motif, CACGTG, was significantly enriched in both ChIP-seq experiments, indicating the robustness of our ChIP-seq assays (q-values < 1e−4; **Fig. 1A**). To identify genes whose transcription was regulated by MYC, we performed cDNA microarray analysis on OVCAR3 and MCF7 cells following RNAi-mediated MYC knockdown. In MCF7 cells, MYC knockdown achieved persistent and efficient (greater than 50%) reduction efficiency. However, despite several attempts, knockdown efficiency in OVCAR3 was not as robust, likely due to the high copy number of *MYC* amplification in this cell line. Therefore, to discover MYC direct target genes, we performed integrated MYC ChIP-seq and MYC-regulated cDNA microarray analysis in MCF7 cells following RNAi-mediated MYC knockdown, and validated the resulting candidate MYC direct target genes using a more sensitive method, qRT-PCR, in both OVCAR3 and MCF7 cells (**Fig. 1B**; Supplementary Fig. S1). Validation of these potential MYC target genes by qRT-PCR was performed on both OVCAR3 and MCF7 tumor cells, and the results showed that most of these genes were significantly downregulated by MYC siRNA-mediated silencing (**Fig. 1B**; Supplementary Fig. S1).

By overlaying 2,161 genes differentially expressed in MYC knockdown versus control groups (fold change > 1.3; $P < 0.05$) and MYC ChIP binding events within 200 Kb flanking the transcription start sites, we identified 1,290 genes as putative MYC direct target genes (hypergeometric $P <$ 1e−4; Supplementary Table S1). Previously reported MYC direct target genes including NOTCH1 (29), NME1-NME4 (30), and CAD (31) were among the MYC target genes identified here, suggesting that these MYC downstream effectors are shared among different human cancers.

Importantly, several druggable enzymes in glutamine metabolism, including GLS, the SLC25 mitochondrial solute transporter family (SLC25A10 and SLC25A39), glutathione synthesis (SHMT2), urea cycle (CAD), and nucleoside synthesis (ADSL, RRM2), are among the identified MYC target genes. MYC ChIP-seq tracings of representative target genes and their flanking regions are shown in Supplementary Fig. S2. Among the drug-targetable MYC downstream genes, we focused on mitochondrial glutaminase (GLS1) for further investigation because it is the first key enzyme in the glutaminolysis pathway. Its blockage in principle would inactivate downstream metabolic steps. Moreover, clinical-grade, oral active GLS inhibitors are under clinical consideration, and one of such GLS inhibitors, CB-839, showed satisfactory tolerability and clinical activity in clinical trials. Although the initial microarray demonstrated a 30% reduction in GSL expression, the MYC ChIP-seq peaks at GLS promoter regions colocalized with RNA Pol II, consistent with direct transcriptional regulation by MYC (Supplementary Fig. S3A). Occupancy of MYC at the GLS promoter was further confirmed by ChIP-qPCR, and notable enrichment of MYC occupancy was observed in GLS^{high} OVCAR3 cells but not in GLS^{low} OAW28 cells (Supplementary Fig. S3B; PCR primer sequences shown in Supplementary Table S2).

MYC target genes identified by ChIP-seq have been reported in HeLa and MEF cells (32, 33). Using those published data, we determined whether genes in glutamine metabolism including GLS were also MYC targets. Interestingly, significant MYC binding was identified at GLS promoter regions of HeLa (Supplementary Fig. S3A; ref. 32) and several cell lines reported previously (Supplementary Table S1 in ref. 33). Moreover, RNA Pol II ChIP-seq in MCF7 and

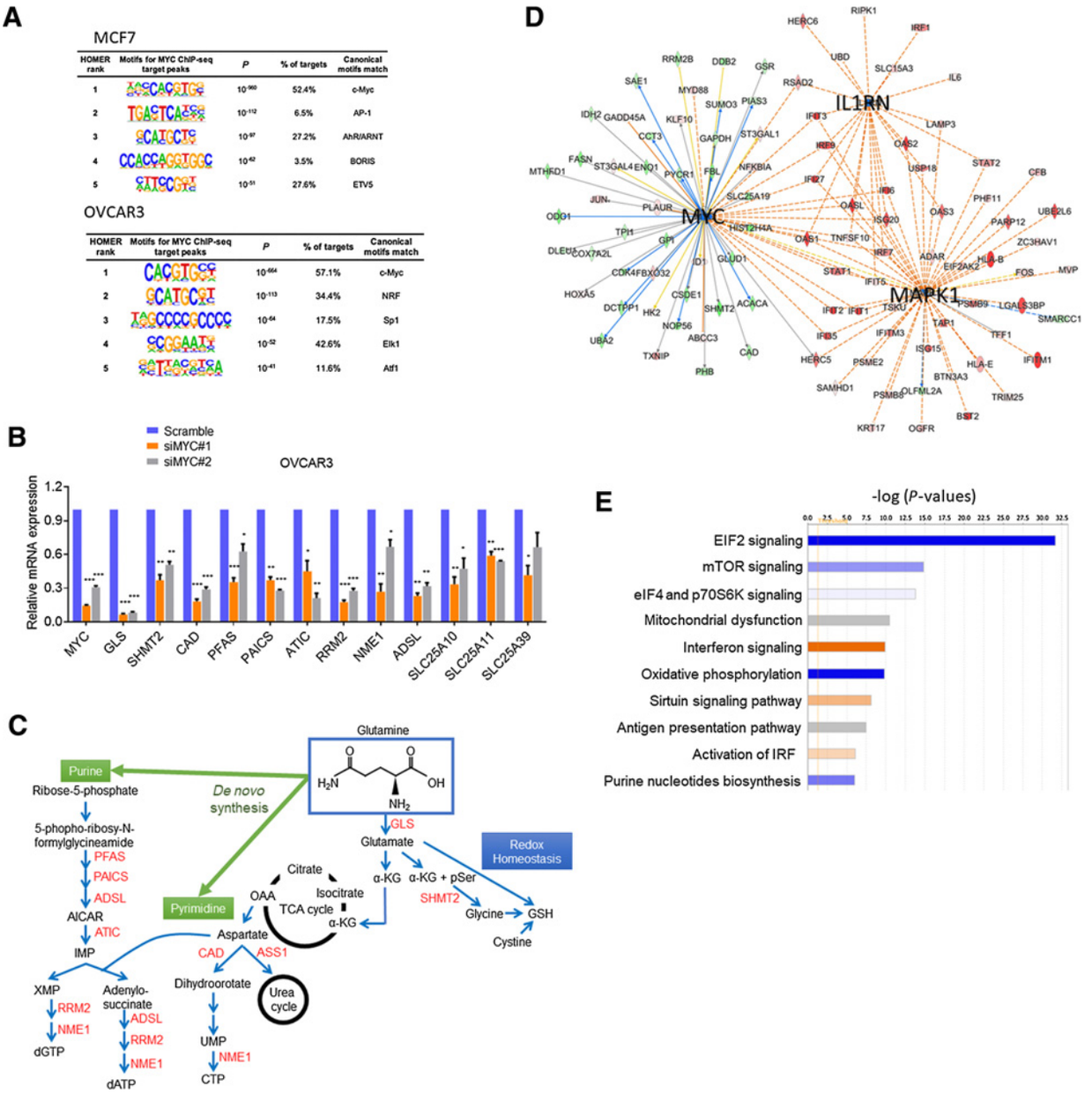

Figure 1.

MYC transcriptionally upregulates genes involved in the glutamine metabolism pathway. **A,** Analysis of MYC ChIP-seq data identifies the highly enriched MYC consensus binding motif as CACGTG. DNA sequences of 200 bp flanking each MYC ChIP-seq peak were extracted from ChIP-seq data of OVCAR3 and MCF7 cells. **B,** Relative mRNA expression levels of MYC and MYC target genes in OVCAR3 following MYC knockdown using two independent siRNAs. Transcription levels of each gene were quantified by RT-qPCR, and data were normalized to a reference gene, APP. Relative expression was further normalized to data obtained from scramble control RNA-treated cells. *, $P < 0.05$; **, $P < 0.01$; ***, $P < 0.001$; $n = 3$, Student t test. **C,** Schema showing MYC-regulated enzymes that are involved in metabolic pathways. OAA, oxaloacetate; GSH, glutathione; UMP, uridine monophosphate; CTP, cytidine triphosphate; AICAR, aminoimidazole carboxamide ribotide; IMP, inosine 5′-monophosphate; XMP, xanthine monophosphate; dGTP, deoxyguanosine triphosphate. **D,** Ingenuity Pathway Analysis performed on MYC target genes identified by overlaying genes differentially expressed in MYC knockdown cells with genes whose promoters and regulatory regions were bound by MYC. Plots show the top three upstream network hubs and molecules in each network. Molecules indicated in green and red correspond to downregulated and upregulated genes following MYC knockdown, respectively. **E,** Analysis of Ingenuity Pathway Analysis data of canonical pathways showing enrichment in MYC target genes. The x-axis represents the negative log P value. Only the top 10 pathways with the most significant negative values are shown. Blue, red, and gray bars indicate pathway downregulated, upregulated, or unregulated in response to MYC knockdown.

HeLa showed Pol II binding sites close to the MYC binding peaks at the GLS promoter, suggestive of cotranscriptional regulation of GLS (Supplementary Fig. S3A). Analysis of MYC target genes in HeLa cells further indicated that several genes in the glutamine metabolism pathway, including SHMT2, PFAS, RRMT2, NME1, and PAICS, were also MYC targets in HeLa. ChIP-seq peaks at promoter regions of these genes are presented in Supplementary Fig. S2. The results suggest that the governess of glutamine metabolism by MYC is likely a conserved transcriptional regulatory program. A schema delineating branches of glutamine metabolic flux containing putative MYC target genes reported in this study is shown in **Fig. 1**C. Using Ingenuity Pathway Analysis performed on the MYC target genes, upstream transcriptional network hubs including MYC, ILIRN, and MAPK1 were identified (**Fig. 1D**). Ingenuity Pathway Analysis also indicated that MYC knockdown resulted in significant downregulation of EIF2, mTOR, and *de novo* purine synthesis canonical pathways (**Fig. 1E**). On the other hand, MYC knockdown unregulated the interferon signaling pathway (**Fig. 1E**).

Elevated MYC and glutaminase in ovarian carcinomas

Based on the experimental evidence that GLS transcription can be regulated directly by MYC (34, 35), we evaluated coexpression of GLS and MYC proteins by IHC in a cohort of 130 ovarian high-grade serous carcinomas (HGSC), 37 ovarian low-grade serous carcinomas (LGSC), and 69 ovarian clear cell carcinomas (OCCC). GLS expression was also evaluated in 22 normal tissue samples, including 8 fallopian tube tissues and 14 endometrial tissues. Representative photomicrographs of GLS and MYC immunostaining are shown in **Fig. 2**A. MYC and GLS H-scores in ovarian cancers were significantly higher than those in normal tissues (**Fig. 2B**; $P < 0.001$). The GLS H-score was significantly higher in HGSC patients than in other histologic subtypes (**Fig. 2B**). Moreover, there was a significant correlation between GLS H-score and MYC H-score in OCCC but not in ovarian HGSC or LGSC (Pearson correlation coefficient $r = 0.4004$, $P < 0.001$ for OCCC; **Fig. 2C**).

We next evaluated GLS and MYC protein expression by Western blot analysis in an expanded panel of cell lines including immortalized cells and primary cultures derived from human female reproductive tract epithelium and ovarian serous or clear cell carcinoma cell lines. We observed that most of the ovarian cancer lines manifested elevated endogenous GLS and MYC expression compared with cells derived from normal epithelium of human female reproductive tract (**Fig. 2D**). GLS expression positively correlated with MYC expression in these ovarian cell lines (**Fig. 2C**; $r = 0.4343$, $P = 0.0301$). Furthermore, knockdown of MYC by two independent siRNAs markedly reduced GLS protein expression in MYC/GLS^{high} cell lines including JHOC-5, OVTOKO, and ES-2, indicating that MYC regulates GLS expression in these cells (**Fig. 2E**).

Ovarian cancers with elevated GLS expression depend on glutaminolysis for cell survival and are associated with platinum resistance

Development of resistance to carboplatin is a major obstacle to achieving long-term remission of ovarian cancer. To assess putative correlation of MYC and GLS expression with resistance, we performed IHC using antibodies specific to MYC or GLS in a cohort of primary and chemoresistant/recurrent ovarian cancers derived from individual patients (**Fig. 3A**). A significant increase in expression levels of GLS protein was identified in resistant tumors compared with primary tumors in a cohort of 31 patients (**Fig. 3B**, $P < 0.001$). However, recurrent tumors did not upregulate MYC in comparison with primary tumors from the same patients (**Fig. 3B**), implying that the MYC regulatory loop may be enriched in only a subset of primary and recurrent tumors. We further analyzed GLS protein levels in ovarian tumor ascites from women treated with platinum-based chemotherapy and found that GLS overexpression (based on a cutoff of 100 in IHC score) was associated with worse disease outcomes, indicated by shorter overall survival than patients with low GLS expression ($P = 0.049$; **Fig. 3C**).

To gain insight into the relationship between GLS overexpression and resistance to platinum-based therapy, we tested carboplatin sensitivity on a panel of ovarian cancer cell lines growing in 3D culture (36). GLS^{high} cells were more resistant to carboplatin compared with GLS^{low} cells, and there was a positive correlation between carboplatin IC_{50} and cellular GLS expression levels (**Fig. 3D**; $r = 0.6986$, $P < 0.001$). We then tested MYC and GLS protein expression in an isogenic pair of carboplatin-resistant (CR) and parental naïve ovarian cancer cell lines, OVCAR8-CR and OVCAR8, and found a concomitant upregulation of GLS and MYC in platinum-resistant CR cells (**Fig. 3E**). These results provide further evidence of an association between upregulation of the MYC/GLS axis and carboplatin resistance.

Inhibition of GLS by CB-839 induces replication stress

To determine whether inhibiting GLS would suppress proliferation of ovarian cancer cells, we treated ovarian cancer cells with CB-839, an orally active, noncompetitive inhibitor of GLS1, which has demonstrated a favorable safety profile in clinical trials (37). We observed that GLS^{high} cells were more sensitive to CB-839 than to GLS^{low} cells (**Fig. 4A**). Interestingly, CB-839 treatment induced poly ADP-ribosylation (PARylation) in GLS^{high} ES-2 and SKOV3 cells, indicating that these cell lines may have induced DNA damage following exposure to CB-839 (**Fig. 4B**). BRCA1 and BRCA2 mutational status was available in cBioPortal for all cell models studied except for OV2008. Both genes were wild-type in all tested cell lines. Because unrepaired DNA damage lesions or imbalanced nucleotide pools eventually cause replication stress when cells enter the replication phase, we examined the effects of CB-839 on the expression of replication stress response markers, pRPA, γH2AX, and pATR. By Western blot analysis, we found that CB-839 potently increased levels of the replication stress markers (**Fig. 4B**, lanes 2 and 8). Importantly, increased levels of γH2AX, pRPA, pATR, and PARylation were abated by supplementing culture medium with dimethyl-α-ketoglutarate (DM-KG), a cell-permeable precursor of α-ketoglutarate (αKG), which is a key metabolite of the glutaminolysis pathway (**Fig. 4B**, lanes 3 and 9). Supplementing the cell culture medium with the ROS neutralizer N-acetylcysteine (NAC) partially alleviated replication stress (**Fig. 4B**, lanes 4 and 10), and supplementation with nucleosides slightly alleviated replication stress (**Fig. 4B**, lanes 5 and 11), suggesting that CB-839 treatment affects the antioxidant and nucleoside synthesis metabolic steps outlined in **Fig. 1**C.

We next investigated whether glutamine depletion would elicit an effect similar to pharmacological inhibition of GLS. GLS^{high} ES-2 cells and GLS^{low} OV2008 cells were cultured in glutamine-depleted medium for 48 hours. Western blot analysis demonstrated an increased PARPylation in ES-2 cells as compared with GLS^{low} OV2008 cells (**Fig. 4C**, lane 1). Although glutamine replenishment in culture medium reversed this phenomenon (**Fig. 4C**, lane 2), the effect was counteracted by CB-839 (**Fig. 4C**, lane 3). Replenishing αKG also significantly rescued nucleotide levels from CB-839 inhibition (**Fig. 4D**). Furthermore, replenishing DM-KG or NAC, the downstream metabolites of the GLS pathway, abated

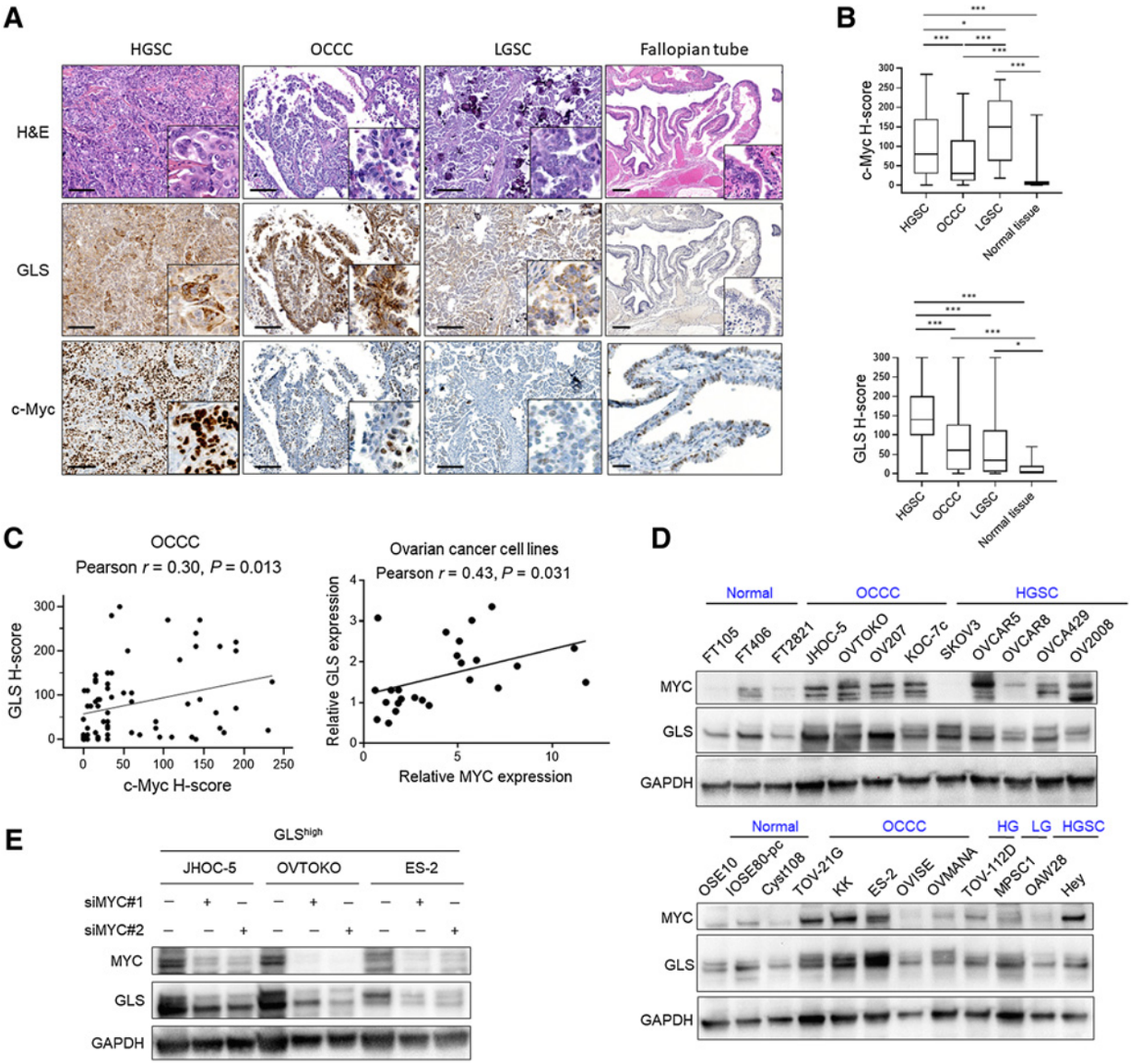

Figure 2.

Correlation of MYC and glutaminase expression levels in ovarian carcinomas. **A,** Representative photomicrographs of GLS and MYC immunoreactivity in HGSC, LGSC, OCCC, and normal fallopian tube. Insets are magnified images. Scale bars, 200 μm. H&E, hematoxylin and eosin. **B,** MYC (top) and GLS (bottom) H-scores in 130 HGSCs, 37 LGSCs, 69 OCCCs, and 22 normal fallopian tube tissues. *, $P < 0.05$; ***, $P < 0.001$; Mann–Whitney test. **C,** Pearson correlation analysis of GLS and MYC expression in OCCC tissues (left) and in ovarian cell lines (right). **D,** Western blot analysis of GLS and MYC protein expression in a panel of nontumorigenic and malignant epithelial cell lines. The nontumorigenic lines include fallopian tube epithelium (FT), ovarian surface epithelium (OSE), cyst, ovarian cystadenoma. GAPDH served as the loading control. **E,** MYC knockdown using two independent siRNAs (siRNA#1 and siRNA#2) on GLS^{high} ovarian cancer cell lines. MYC knockdown efficiency and the effect on GLS expression are evaluated by Western blot analysis. GAPDH served as an internal loading control.

CB-839–induced increase in both intracellular and mitochondrial ROS levels (**Fig. 4E**).

The GLS inhibitor CB-839 is a potent PARPi sensitizer

Replication stress elicited by CB-839 may cause cells to rely on PARP-dependent replication fork repair to facilitate progression of DNA replication and completion of the cell cycle. Therefore, we postulated that GLS inhibition would enhance sensitivity of tumor cells to PARP inhibitor, leading to fork collapse, DNA double strand breaks (DSB), and subsequent cell death. To test this possibility, we measured the combination index using the Chou–Talalay method to evaluate whether combined treatment with CB-839 and olaparib would achieve a synergistic antitumor activity. As shown in **Fig. 5A**, we observed a synergistic effect of the combination in GLS^{high} cells. As predicted, combined CB-839 and olaparib treatment in GLS^{high} cells significantly increased DSBs as evidenced by enhanced γH2AX levels compared with single-agent treatment (**Fig. 5B**). In contrast, GLS^{low} cells responded well to olaparib applied as a single agent, but no further effects were observed when CB-839 was combined with the olaparib treatment.

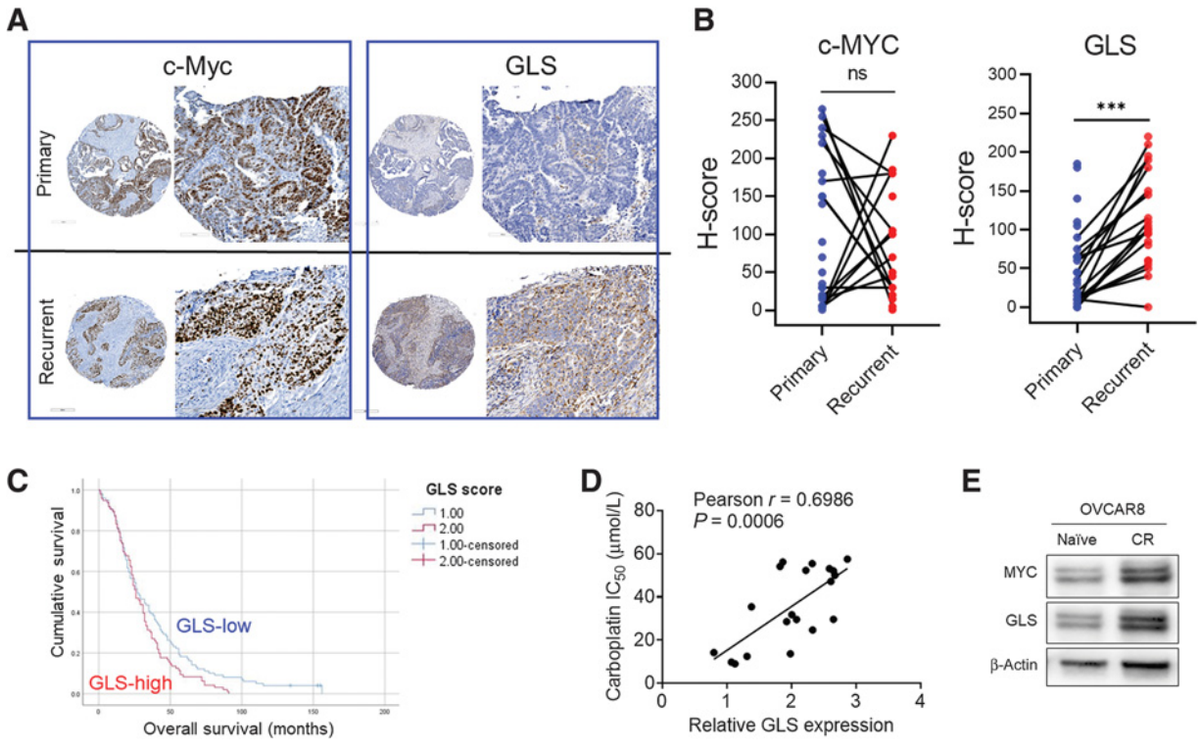

Figure 3.

Elevated GLS expression in recurrent/chemoresistant ovarian carcinomas. **A,** Representative photomicrographs of MYC and GLS IHC staining in primary and recurrent ovarian carcinoma tissues from the same patient. **B,** H-scores of matched primary and recurrent ovarian cancers from 31 women. Recurrent tumors had elevated GLS H-scores as compared with primary tumors (***, $P < 0.001$, paired t test). There was no significant (ns) difference in MYC expression between primary and recurrent ovarian cancers from the same patients (paired t test). **C,** Univariate survival analysis on GLS expression in tumors collected from 195 ovarian cancer patients who had received platinum-based chemotherapy at diagnosis. Patients were stratified into GLS^{high} ($n = 99$) and GLS^{low} ($n = 96$) groups. GLS^{high} patients had shorter overall survival than GLS^{low} patients, with mean overall survival of 31 vs. 39 months, respectively ($P = 0.049$, log-rank test). **D,** Pearson correlation analysis of carboplatin sensitivity (IC_{50} of carboplatin) and relative GLS levels in ovarian cancer cell lines ($r = 0.6986$, $P = 0.0006$). **E,** Western blot analysis of MYC and GLS protein expression in OVCAR8-naïve and CR cells. β-Actin served as an internal control.

To verify this finding, we knocked down GLS in GLS^{high} cells and found that attenuation of GLS expression (**Fig. 5C**), similar to CB-839 treatment, potently sensitized GLS^{high} cells to olaparib (**Fig. 5D**). Importantly, the synergistic cytotoxicity of CB-839 and olaparib was fully abrogated by the addition of DM-KG (a cell-permeable form of αKG) to the culture medium (**Fig. 5E**), results strongly supporting that GLS inhibition suppresses the downstream metabolite, αKG, and αKG–mediated functions.

CB-839 affects the intracellular redox state and disturbs the balance of GSH/GSSG

To further assess the mechanism by which CB-839 alters the intracellular redox state, we quantified the ratio of reduced and oxidized glutathione (GSH/GSSG), and measured intracellular ROS and mitochondrial superoxide by CellROX green and MitoSOX, respectively, in ovarian cancer cells treated with CB-839 alone or in combination with olaparib. It is well known that GSH neutralizes ROS and protects cells from oxidative stress, and that the GSH/GSSG ratio reflects the intracellular redox status. We found that GLS^{high} cells had higher intrinsic GSH/GSSH ratios than GLS^{low} cells (Supplementary Fig. S4A). We also directly measured intracellular ROS levels and found that GLS^{high} cells harbor concomitantly reduced levels of ROS and mitochondrial superoxide (MitoSOX) compared with GLS^{low} cells (Supplementary Fig. S4B). In GLS^{high} cells, CB-839 decreased the GSH/GSSH ratio and stimulated both intracellular and mitochondrial ROS levels (Supplementary Fig. S4C and S4D). The combination of olaparib and GLS inhibitor led to a further reduction of the GSH/GSSH ratio and of both ROS and MitoSOX levels in GLS^{high} cells, but not in GLS^{low} cells (Supplementary Fig. S4C and S4D).

To determine whether GLS levels were associated with cellular dependence on glutaminolysis, which can be used as a biomarker for predicting treatment response to GLS inhibitor, we measured the viability of ovarian cancer cells grown in 3D culture systems with glutamine-depleted or glucose-depleted culture medium. GLS^{high} cells were more sensitive to glutamine deprivation than GLS^{low} cells (Supplementary Fig. S4E). Conversely, GLS^{high} cells were less sensitive to glucose depletion than GLS^{low} cells (Supplementary Fig. S4E), suggesting that GLS^{high} tumor cells, which have elevated GLS levels, may utilize a metabolic program different from GLS^{low} cells.

In vivo therapeutic efficacy of the GLS inhibitor CB-839 in combination with PARP inhibitor

The *in vitro* data presented above suggest that GLS^{high} cancer cells adopt a transcriptomic-metabolic program that promotes glutamine utilization for generating antioxidants and synthesizing nucleosides. The data also suggest that this unique metabolic program in GLS^{high} cancer cells can be exploited for targeted cancer treatment. To assess this possibility, we evaluated the *in vivo* efficacy of CB-839 for

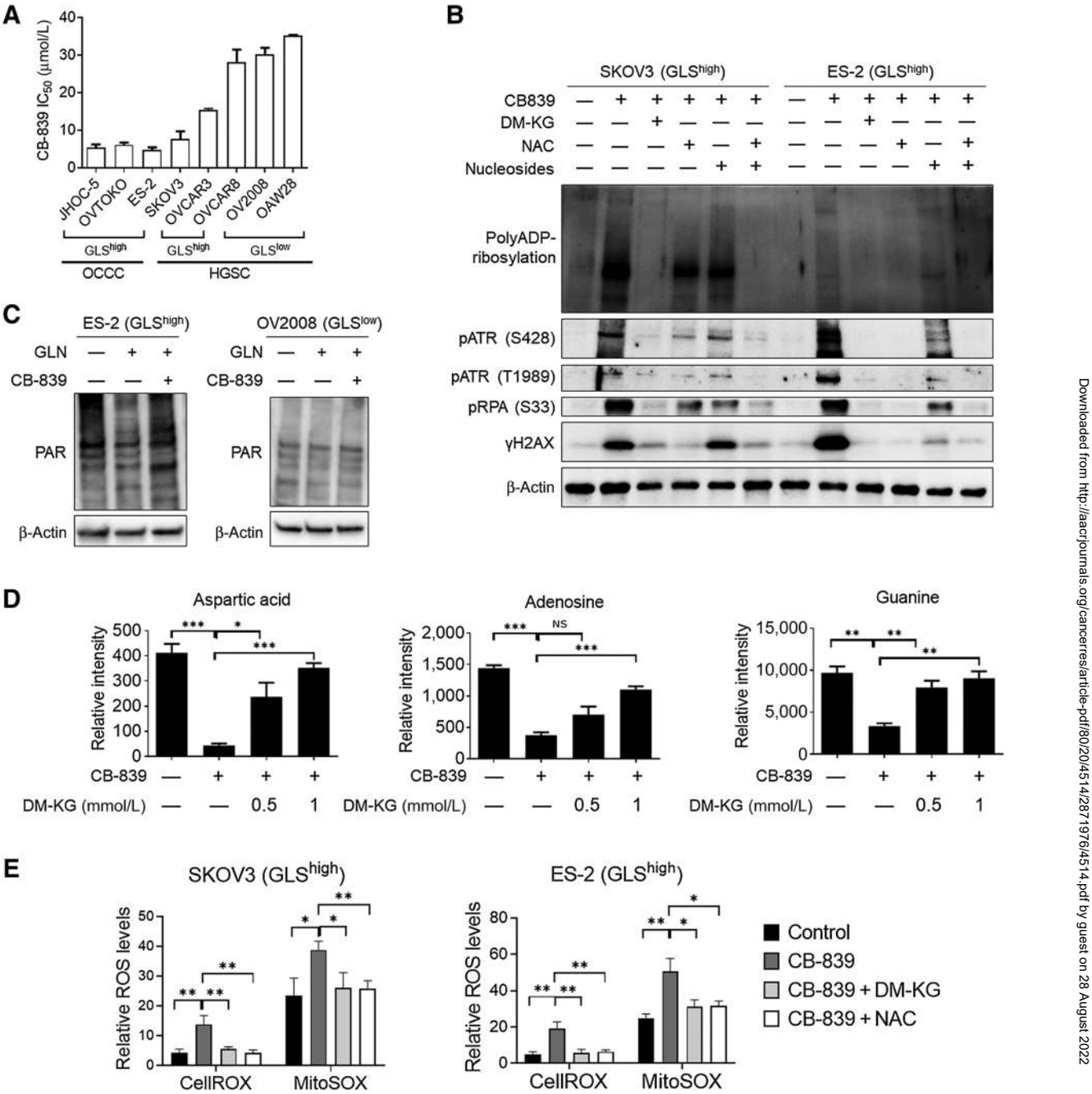

Figure 4.

Inhibition of GLS by CB-839 induces oxidative and replication stress. **A,** IC_{50} of CB-839 in different ovarian cancer cell lines exhibiting various GLS expression levels. Data, mean ± SEM of triplicate experiments. **B,** Western blot analysis of PAR polymer, pATR (pS428), pATR (pT1989), pRPA (pS33), and γH2AX in SKOV3 and ES-2 cells treated with CB-839 (2.5 μmol/L), DM-KG (1 mmol/L), NAC (4 mmol/L), and/or nucleosides (5 μmol/L). DM-KG, dimethyl-α-ketoglutarate, a cell-permeable precursor of α-ketoglutarate; NAC, N-acetylcysteine, precursor for the biosynthesis of glutathione, a major antioxidant in cells. **C,** Western blots of PAR polymer protein expression in ES-2 (GLS^{high}; left) and OV2008 (GLS^{low}; right) with or without glutamine depletion, and in the presence or absence of CB-839 (2.5 μmol/L). β-Actin served as an internal control. **D,** Levels of nucleotide precursors, aspartate, adenosine, and guanine, measured by a triple-quadrupole mass spectrometer in SKOV3 cells treated with indicated compounds. The level of each nucleotide precursor was normalized to total protein concentration to obtain relative intensity. **E,** Intracellular ROS and mitochondrial ROS levels were measured by CellROX green and MitoSOX, respectively, in SKOV3 cells (left) and ES-2 cells (right) treated with 2.5 μmol/L CB-839 alone or cotreated with 1 mmol/L DM-KG or 4 mmol/L NAC. *, $P < 0.05$; **, $P < 0.01$; ***, $P < 0.001$; NS, not statistically significant; Student t test.

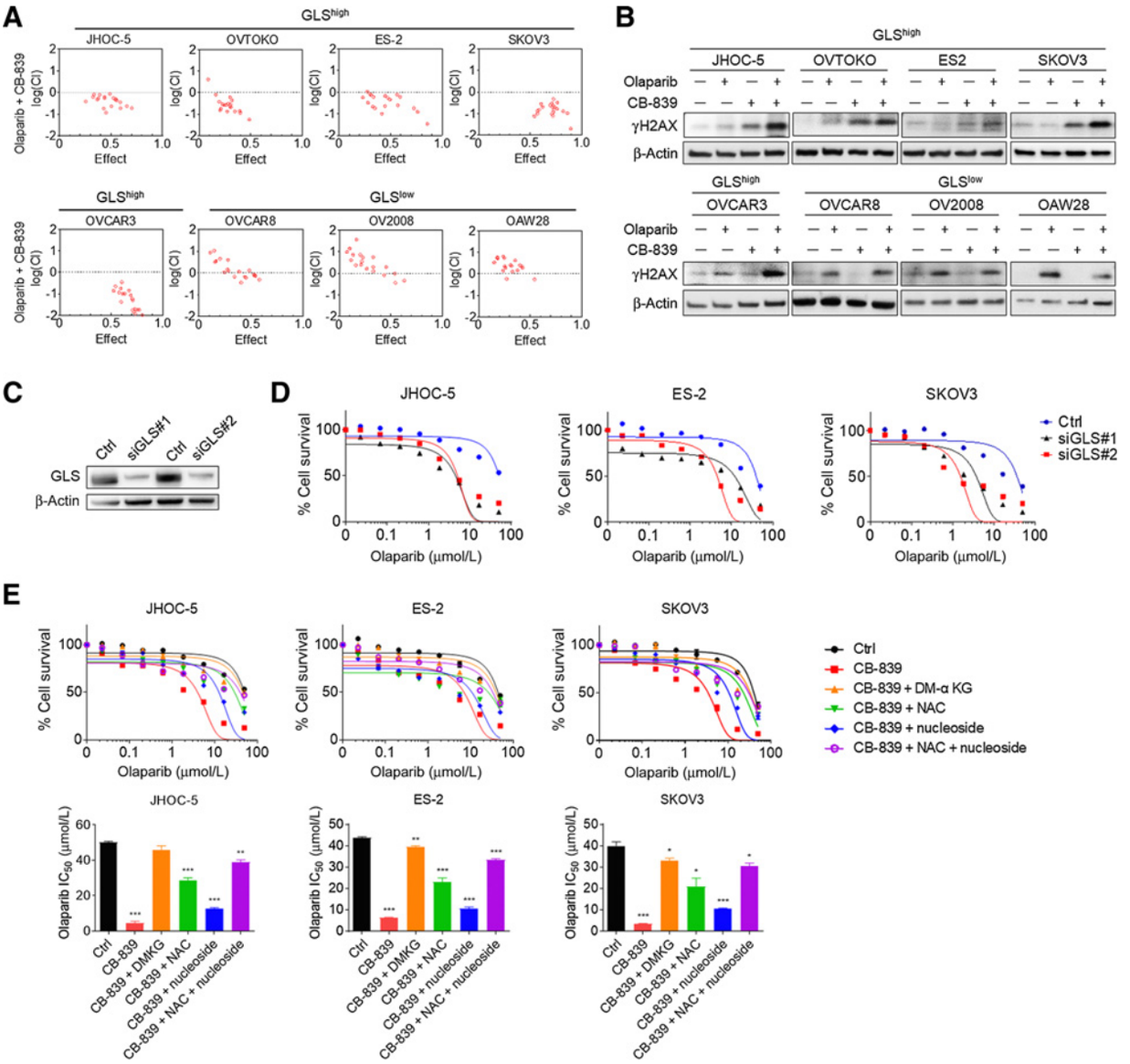

Figure 5.

PARP inhibitor sensitizes GLS^{high} cells to GLS inhibition. **A,** Effect of the combination of CB-839 and olaparib in ovarian cancer cell lines analyzed by CompuSyn. Symbols represent individual combination index (CI) values at 20 different drug combination doses. **B,** Western blot analysis of γH2AX expression in ovarian cancer cells with indicated treatment. β-Actin served as an internal control. **C,** Western blot analysis of GLS knockdown efficiency in ES-2 cells (GLS^{high}) with two independent siRNAs (siGLS#1 and #2). β-Actin served as an internal control. **D,** Cell survival analysis performed on GLS^{high} cancer cell lines, JHOC-5, ES-2, and SKOV3, grown in a 3D culture system. Cells were pretreated with GLS siRNAs and then incubated with various concentrations of olaparib. **E,** GLS^{high} cancer cells growing in the 3D culture system were treated with CB-939 in combination with various doses of olaparib to determine the IC_{50} of olaparib. Metabolites downstream of GLS, including DM-KG, NAC, and nucleosides, were added to the culture medium to evaluate rescue effects. Data, mean ± SEM of triplicate wells. *, $P < 0.05$; **, $P < 0.01$; ***, $P < 0.001$; ns, not statistically significant; Student *t* test.

sensitizing GLS^{high} ES-2 and SKOV3 ovarian tumor xenografts to olaparib in athymic *nu/nu* mice. As a comparison, the same experiments were performed on GLS^{low} OV2008 tumor xenografts. When subcutaneous tumor xenografts reached approximately 100 mm^3, mice were randomized and treated with CB-839, olaparib, vehicle control, or a combination of CB-839 and olaparib. CB-839 as a single agent modestly delayed the progression of GLS^{high} ES-2 and SKOV3 tumors (**Fig. 6A**; Supplementary Fig. S5A and S5B). Addition of olaparib to the regimen significantly enhanced antitumor efficacy in these two GLS^{high} tumor models (**Fig. 6A**; Supplementary Fig. S5A and S5B). At the endpoint, CB-389 significantly decreased the size of ES-2 (GLS^{high}) but not OV2008 (GLS^{low}) tumors ($P < 0.01$). On the other hand, olaparib significantly decreased the growth in OV2008 tumor but not in ES-2 tumor ($P < 0.001$). Increased survival was observed in mice with ES-2 tumors that had been treated with the combination regimen (**Fig. 6B**). In contrast, GLS^{low} OV2008 tumors responded well

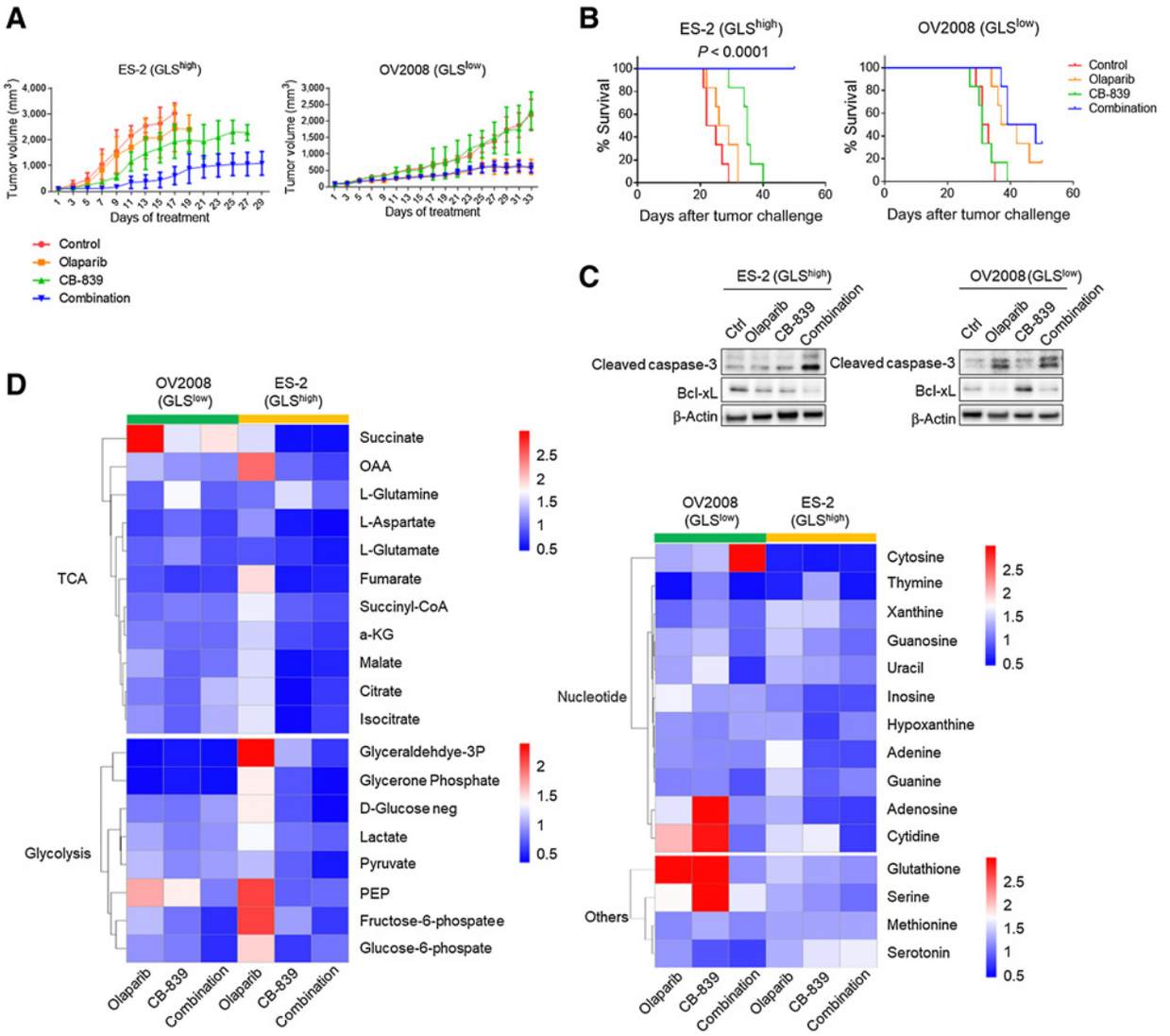

Figure 6.

Antitumor efficacy of GLSi and PARPi combination treatment in xenograft models of ovarian cancer. **A,** Immunocompromised athymic *nu/nu* mice were inoculated with human ovarian cancer cells, ES-2 (GLS^{high}) and OV2008 (GLS^{low}). Mice bearing established tumors were randomized into four different treatment groups: CB-839 only, olaparib only, CB-839 + olaparib, and control vehicle. Tumor volume was monitored every other day. Differences in tumor growth were analyzed by Student *t* test. $n = 6$ for each treatment group. **B,** Kaplan–Meier survival curves for mice bearing ES-2 or OV2008 xenograft tumors. Log-rank test, $n = 6$ for each group. **C,** Western blots of the apoptotic marker, cleaved caspase-3, and the antiapoptotic marker, Bcl-xL, in ES-2 and OV2008 tumor xenografts excised from mice in different treatment groups. β-Actin served as an internal control. **D,** Heat map showing levels of metabolites in glutaminolysis and glycolysis pathways from lysates of xenografted tumors prepared from mice treated with indicated drug or a combination of drugs. Metabolites are presented in four groups: TCA cycle, glycolysis, nucleotides, and others. The data are normalized to data obtained from mice treated with vehicle control.

to olaparib as a single agent, but not to CB-839; furthermore, addition of CB-839 to olaparib had no further effect on GLS^{low} OV2008 tumors, nor did it improve survival (**Fig. 6A** and **B**). We also observed an increase in cleaved caspase-3 and a decrease in BCL-XL expression in GLS^{high} ES-2 tumors treated with CB-839 and olaparib together. In GLS^{low} OV2008 tumors, olaparib alone was sufficient to cause apoptosis (**Fig. 6C**). The data were further confirmed by IHC. Supplementary Fig. S6 shows the percentage of positive tumor cells in xenograft tumors treated with different drug(s), and representative images of cleaved caspase-3 immunoreactivity are shown.

To determine whether treatment of CB-839 induces replication stress *in vivo*, IHC using an antibody against pRPA was performed on the same cohort of xenograft tumors treated with different drug(s). The data indicate a significant upregulation of pRPA in CB-839–treated GLS^{high} xenograft tumors, ES-2 and SKOV3, but not in CB-839–treated GLS^{low} OV2008 tumors. In SKOV3 xenografts, olaparib single-agent treatment also induces pRPA expression. Comparison of H-scores and representative images of its immunoreactivity in xenograft tumors are shown in Supplementary Fig. S7.

To gain insight into the *in vivo* biological effects of CB-839, we performed quantitative LC-MS mass spectrometry to measure

metabolites in tumor xenografts. Each metabolite from drug-treated groups was normalized to total protein, and was then compared with the same metabolite from vehicle control-treated tumor xenografts. Differential expression levels are presented in a color-coded heat map (**Fig. 6D**), with red indicating the greatest abundance and blue indicating the lowest abundance. CB-839–treated GLS^{high} tumors had elevated glutamine and reduced glutamate levels, indicating that *in vivo* inhibition of GLS by CB-839 resulted in the accumulation of glutamine. Key metabolites in the glutaminolysis pathway including αKG and citrate were significantly reduced in CB-839–treated GLS^{high} tumors whether the drug was given as a single agent or in combination with olaparib (**Fig. 6D**). We also measured inosine, adenine, and guanine in the purine *de novo* synthesis pathway and L-aspartate, which donates a nitrogen to the purine base. Due to the concern that pyrimidine nucleotides can be confounded by excess urea/uridine in the biology system, we did not assess the pyrimidine *de novo* synthesis pathway. In GLS^{high} tumors, the levels of purine nucleotides, including inosine, adenine, guanine, and L-aspartate, were significantly affected by CB-839 treatment (**Fig. 6D**; Supplementary Fig. S8). The data collectively indicate that CB-839 treatment effectively suppresses glutamine metabolism *in vivo*.

Discussion

In this study, we found that ovarian cancer cells reprogram the glutamine-mediated metabolic pathway in response to upregulation of the MYC/GLS transcription axis. We demonstrated that inhibiting MYC-regulated GLS upregulated replication stress markers and sensitizes GLS-overexpressing ovarian cancer cells to PARP inhibitors. Because upregulation of MYC and/or GLS is often associated with resistance to chemotherapy and worse clinical prognosis in cancer patients, the findings reported here not only enhance our understanding of the chemoresistance mechanism but may also be applicable to future cancer treatment strategies.

The integrated MYC ChIP-seq and MYC-regulated transcriptome analysis of human cancer cells yielded an array of MYC target genes including GLS. Aside from GLS, previously unidentified or less known MYC-regulated genes such as SHMT2, SLC25A10, and SLC25A35 in regulating redox balance were also reported here. SHMT2 catalyzes the conversion of serine to glycine plus a tetrahydrofolate-bound single-carbon unit, which subsequently facilitates glutathione and nucleotide synthesis, mitochondrial NADPH generation, and mitochondrial redox balance during hypoxia (38). SLC25A10 and SLC25A35 belong to the mitochondrial solute transporter family and are critical for maintaining redox balance and preventing oxidative stress (39). Because MYC activity contributes to the aggressive nature of human cancers, it is likely that transcriptional upregulation of these MYC target genes promotes redox balance, increases intracellular macromolecular supply, enhances nucleotide production, and prevents oxidative stress. These MYC-regulated genes likely work in concert to promote tumor cell fitness in response to environmental challenges such as oxygen and nutrient deprivation, lactic acidosis, immunosurveillance, and clinical treatments.

Coexpression of MYC and GLS occurred in a subset of ovarian carcinomas and ovarian cancer cell lines. Among the three tested histologic types of ovarian carcinomas, OCCCs exhibit most significant co-upregulation of MYC and GLS, whereas recurrent HGSCs did not, indicating that the MYC/GLS coregulatory loop is tissue-type or context-specific. It is likely that in certain contexts, other transcription mechanisms may directly regulate GLS or may work with MYC to comodulate GLS expression. MYC consistently upregulated GLS in the three cell lines established from primary OCCCs (**Fig. 2E**), supporting the dominant role of this transcription regulatory loop in some ovarian cancers. Our finding that MYC occupied and colocalized with RNA polymerase II at the GLS upstream regulatory region in mammalian cell lines indicates a conserved feature of this transcription regulation.

In the current study, GLS overexpression was associated with treatment failure in a significant fraction of recurrent ovarian cancers pretreated with platinum chemotherapy (**Fig. 3A–C**). The widely used platinum-based chemotherapeutic drugs induce reactive oxygen species and the collapse of the DNA replication fork in cancer cells (40, 41). GLS^{high} ovarian cancer cells are likely to show better survival when exposed to platinum drugs, as they utilize GLS and its regulated metabolism to defend themselves from potential oxidative damage and to overcome replication stress. Experimental results demonstrated that GLS inhibition repressed the generation of antioxidant GSH and affected the synthesis of nucleotides, resulting in elevated oxidative stress and DNA replication stress in GLS^{high} cells. Increased understanding of this mechanism suggests the potential for the development of a rational treatment for GLS^{high} ovarian cancers using GLS inhibitor to sensitize resistant tumors. The observations here support recent reports showing that a nonclinical-grade GLS inhibitor BPTES inhibits DNA replication and growth of a MYC-dependent human B cell lymphoma cell line (42), and induces nucleoside depletion, reactive oxygen species, and DNA replication stress in VHL$^{-/-}$ RCC cells (43).

A clinically relevant observation made here is that CB-839, an oral active GLS inhibitor currently being evaluated in clinical trials, has potent anticancer efficacy for GLS^{high} ovarian cancers, especially when combined with the PARP inhibitor, olaparib. We postulate that inhibiting PARP1 is insufficient to kill ovarian tumor cells unless these cells are overwhelmed with replication stress induced by GLS inhibition. Supporting this view, CB-839 was shown to potently suppress the production of α-ketoglutarate, a metabolite at the crossroads of reductive carboxylation and the TCA cycle, acting upstream of the glutathione and nucleotide synthesis pathways. As a result, inhibition of GLS compromises redox homeostasis in favor of oxidative stress and reduces nucleotide pools. Although PARP inhibitors have been clinically used for treating ovarian cancers, mostly in patients with BRCA mutation (44), the efficacy of PARP inhibitor given as a single agent varies among patients, and a significant fraction of patients develop acquired resistance after initial treatment (45). Our experimental results suggest that the clinical benefit of PARP inhibitors can be further enhanced by combining it with metabolic inhibitors such as CB-839. This finding is conceptually in agreement with our recent finding that the efficacy of PARP inhibitors was significantly enhanced when ARID1A-deficient tumors were primed with radiation-induced DNA damages that could not be efficiently repaired (46).

To facilitate future clinical applications of GLSi-based cancer therapy, an immediate task is to perform comprehensive assessment of the dose range and safety profiles. Future studies are also needed to evaluate the range of tumors in which synergistic antitumor effects can be observed and to characterize biomarkers that can identify patients who are most likely to benefit from GLSi-based treatment. Considering the basic mechanism of tumor biology and drug resistance, it can be rewarding to explore the roles of other targetable enzymes in the MYC axis and to test the efficacy of cotargeting MYC downstream genes/pathways. For example, MYC target genes are enriched in mTOR signaling and redox balance pathways. The data provide molecular basis for a clinical trial applying GLS and mTOR cotargeting strategy (NCT03163667) and

support the concept of combining CB-839 and a PARPi, talazoparib, for treating solid tumors (NCT03875313). The data presented here should motivate efforts to simultaneously target cancer metabolism and DNA damage repair to improve clinical outcomes in women with recurrent chemoresistance ovarian cancer, who unfortunately have limited treatment options.

Disclosure of Potential Conflicts of Interest

A.M. DeMarzo reports personal fees from Cepheid (consulting fees) and grants from Janssen R&E and Myriad Genetics (sponsored research) outside the submitted work. S. Gaillard reports grants and personal fees from AstraZeneca, personal fees from Immunogen and Sermonix, and grants from AbbVie, Pfizer, Rigel, Iovance, Tesaro, and Genentech/Roche outside the submitted work; in addition, S. Gaillard has a patent for PCT/US2019/026669 licensed to Sermonix. No potential conflicts of interest were disclosed by the other authors.

Authors' Contributions

Y.-A. Shen: Data curation, formal analysis, validation, investigation, writing–original draft, writing–review, and editing. **J. Hong:** Data curation, validation, and investigation. **R. Asaka:** Data curation, formal analysis, validation, and investigation. **S. Asaka:** Data curation, validation, and investigation. **F.-C. Hsu:** Software, formal analysis, validation, and investigation. **Y. Suryo Rahmanto:** Validation and investigation. **J.-G. Jung:** Validation and investigation. **Y.-W. Chen:** Data curation and investigation. **T.-T. Yen:** Investigation. **A. Tomaszewski:** Data curation, software, formal analysis, and investigation. **C. Zhang:** Data curation, software, formal analysis, and investigation. **N. Attarwala:** Data curation, software, and investigation. **A.M. DeMarzo:** Supervision, validation, writing–review, and editing. **B. Davidson:** Data curation, formal analysis, validation, writing–review, and editing. **C.-M. Chuang:** Supervision, funding acquisition, writing–review, and editing. **X. Chen:** Software, formal analysis, validation, writing–review, and editing. **S. Gaillard:** Supervision, validation, writing–review, and editing. **A. Le:** Software, validation, writing–review, and editing. **I.-M. Shih:** Supervision, validation, writing–original draft, writing–review, and editing. **T.-L. Wang:** Supervision, validation, writing–original draft, writing–review, and editing.

Acknowledgments

The study was supported by NIH grants RO1CA215483, RO1CA148826, P50CA228991, P30CA006973, Ovarian Cancer Research Alliance, and the Johns Hopkins-Allegheny Health Network Cancer Research Fund. We acknowledge Calithera Bioscience (South San Francisco, CA) for providing CB-839 for *in vitro* and *in vivo* studies reported here. We thank Marina Gelman for her critical reading of the manuscript and valuable comments.

The costs of publication of this article were defrayed in part by the payment of page charges. This article must therefore be hereby marked *advertisement* in accordance with 18 U.S.C. Section 1734 solely to indicate this fact.

Received December 26, 2019; revised June 21, 2020; accepted August 25, 2020; published first August 28, 2020.

References

1. Chan JK, Chow S, Bhowmik S, Mann A, Kapp DS, Coleman RL. Metastatic gynecologic malignancies: advances in treatment and management. Clin Exp Metastasis 2018;35:521–33.
2. Prathapam T, Aleshin A, Guan Y, Gray JW, Martin GS. p27Kip1 mediates addiction of ovarian cancer cells to MYCC (c-MYC) and their dependence on MYC paralogs. J Biol Chem 2010;285:32529–38.
3. Yuneva M, Zamboni N, Oefner P, Sachidanandam R, Lazebnik Y. Deficiency in glutamine but not glucose induces MYC-dependent apoptosis in human cells. J Cell Biol 2007;178:93–105.
4. Mohamed A, Deng X, Khuri FR, Owonikoko TK. Altered glutamine metabolism and therapeutic opportunities for lung cancer. Clin Lung Cancer 2014;15:7–15.
5. Altman BJ, Stine ZE, Dang CV. From Krebs to clinic: glutamine metabolism to cancer therapy. Nat Rev Cancer 2016;16:619–34.
6. Shanware NP, Mullen AR, DeBerardinis RJ, Abraham RT. Glutamine: pleiotropic roles in tumor growth and stress resistance. J Mol Med (Berl) 2011;89:229–36.
7. Welbourne TC. Ammonia production and glutamine incorporation into glutathione in the functioning rat kidney. Can J Biochem 1979;57:233–7.
8. DeBerardinis RJ, Mancuso A, Daikhin E, Nissim I, Yudkoff M, Wehrli S, et al. Beyond aerobic glycolysis: transformed cells can engage in glutamine metabolism that exceeds the requirement for protein and nucleotide synthesis. Proc Natl Acad Sci U S A 2007;104:19345–50.
9. Son J, Lyssiotis CA, Ying H, Wang X, Hua S, Ligorio M, et al. Glutamine supports pancreatic cancer growth through a KRAS-regulated metabolic pathway. Nature 2013;496:101–5.
10. Botman D, Tigchelaar W, Van Noorden CJ. Determination of phosphate-activated glutaminase activity and its kinetics in mouse tissues using metabolic mapping (quantitative enzyme histochemistry). J Histochem Cytochem 2014;62:813–26.
11. Ulanet DB, Couto K, Jha A, Choe S, Wang A, Woo HK, et al. Mesenchymal phenotype predisposes lung cancer cells to impaired proliferation and redox stress in response to glutaminase inhibition. PLoS One 2014;9:e115144.
12. Yuan L, Sheng X, Willson AK, Roque DR, Stine JE, Guo H, et al. Glutamine promotes ovarian cancer cell proliferation through the mTOR/S6 pathway. Endocr Relat Cancer 2015;22:577–91.
13. Godwin AK, Meister A, O'Dwyer PJ, Huang CS, Hamilton TC, Anderson ME. High resistance to cisplatin in human ovarian cancer cell lines is associated with marked increase of glutathione synthesis. Proc Natl Acad Sci U S A 1992;89:3070–4.
14. Momcilovic M, Bailey ST, Lee JT, Fishbein MC, Magyar C, Braas D, et al. Targeted inhibition of EGFR and glutaminase induces metabolic crisis in EGFR mutant lung cancer. Cell Rep 2017;18:601–10.
15. Chakrabarti G, Moore ZR, Luo X, Ilcheva M, Ali A, Padanad M, et al. Targeting glutamine metabolism sensitizes pancreatic cancer to PARP-driven metabolic catastrophe induced by ss-lapachone. Cancer Metab 2015;3:12.
16. Cai T, Lorenzi PL, Rakheja D, Pontikos MA, Lodi A, Han L, et al. Gls inhibitor CB-839 modulates cellular metabolism in AML and potently suppresses AML cell growth when combined with 5-azacitidine. Blood 2016;128:4064.
17. Jacque N, Ronchetti AM, Larrue C, Meunier G, Birsen R, Willems L, et al. Targeting glutaminolysis has antileukemic activity in acute myeloid leukemia and synergizes with BCL-2 inhibition. Blood 2015;126:1346–56.
18. Li J, Csibi A, Yang S, Hoffman GR, Li C, Zhang E, et al. Synthetic lethality of combined glutaminase and Hsp90 inhibition in mTORC1-driven tumor cells. Proc Natl Acad Sci U S A 2015;112:E21–9.
19. Hudson CD, Savadelis A, Nagaraj AB, Joseph P, Avril S, DiFeo A, et al. Altered glutamine metabolism in platinum resistant ovarian cancer. Oncotarget 2016;7:41637–49.
20. Yuan L, Sheng X, Clark LH, Zhang L, Guo H, Jones HM, et al. Glutaminase inhibitor compound 968 inhibits cell proliferation and sensitizes paclitaxel in ovarian cancer. Am J Transl Res 2016;8:4265–77.
21. Masamha CP, LaFontaine P. Molecular targeting of glutaminase sensitizes ovarian cancer cells to chemotherapy. J Cell Biochem 2018;119:6136–45.
22. Choi JH, Choi KC, Auersperg N, Leung PC. Gonadotropins upregulate the epidermal growth factor receptor through activation of mitogen-activated protein kinases and phosphatidyl-inositol-3-kinase in human ovarian surface epithelial cells. Endocr Relat Cancer 2005;12:407–21.
23. Pohl G, Ho CL, Kurman RJ, Bristow R, Wang TL, Shih Ie M. Inactivation of the mitogen-activated protein kinase pathway as a potential target-based therapy in ovarian serous tumors with KRAS or BRAF mutations. Cancer Res 2005;65:1994–2000.
24. Maeda T, Tashiro H, Katabuchi H, Begum M, Ohtake H, Kiyono T, et al. Establishment of an immortalised human ovarian surface epithelial cell line without chromosomal instability. Br J Cancer 2005;93:116–23.
25. Blayney JK, Davison T, McCabe N, Walker S, Keating K, Delaney T, et al. Prior knowledge transfer across transcriptional data sets and technologies using compositional statistics yields new mislabelled ovarian cell line. Nucleic Acids Res 2016;44:e137.
26. Langmead B, Salzberg SL. Fast gapped-read alignment with Bowtie 2. Nat Methods 2012;9:357–9.

27. Zhang Y, Liu T, Meyer CA, Eeckhoute J, Johnson DS, Bernstein BE, et al. Model-based analysis of ChIP-Seq (MACS). Genome Biol 2008;9:R137.
28. Heinz S, Benner C, Spann N, Bertolino E, Lin YC, Laslo P, et al. Simple combinations of lineage-determining transcription factors prime cis-regulatory elements required for macrophage and B cell identities. Mol Cell 2010;38: 576–89.
29. Sanchez-Martin M, Ferrando A. The NOTCH1-MYC highway toward T-cell acute lymphoblastic leukemia. Blood 2017;129:1124–33.
30. Liu Y-C, Li F, Handler J, Huang CRL, Xiang Y, Neretti N, et al. Global regulation of nucleotide biosynthetic genes by c-Myc. PLoS One 2008;3:e2722.
31. Miltenberger RJ, Sukow KA, Farnham PJ. An E-box-mediated increase in cad transcription at the G1/S-phase boundary is suppressed by inhibitory c-Myc mutants. Mol Cell Biol 1995;15:2527–35.
32. Walz S, Lorenzin F, Morton J, Wiese KE, von Eyss B, Herold S, et al. Activation and repression by oncogenic MYC shape tumour-specific gene expression profiles. Nature 2014;511:483–7.
33. Lin CY, Lovén J, Rahl PB, Paranal RM, Burge CB, Bradner JE, et al. Transcriptional amplification in tumor cells with elevated c-Myc. Cell 2012;151:56–67.
34. Gao P, Tchernyshyov I, Chang TC, Lee YS, Kita K, Ochi T, et al. c-Myc suppression of miR-23a/b enhances mitochondrial glutaminase expression and glutamine metabolism. Nature 2009;458:762–5.
35. Stine ZE, Walton ZE, Altman BJ, Hsieh AL, Dang CV. MYC, Metabolism, and Cancer. Cancer Discov 2015;5:1024–39.
36. Frieboes HB, Zheng X, Sun CH, Tromberg B, Gatenby R, Cristini V. An integrated computational/experimental model of tumor invasion. Cancer Res 2006;66:1597–604.
37. Xu X, Meng Y, Li L, Xu P, Wang J, Li Z, et al. Overview of the development of glutaminase inhibitors: achievements and future directions. J Med Chem 2019; 62:1096–115.
38. Ye J, Fan J, Venneti S, Wan YW, Pawel BR, Zhang J, et al. Serine catabolism regulates mitochondrial redox control during hypoxia. Cancer Discov 2014;4: 1406–17.
39. Zhou X, Paredes JA, Krishnan S, Curbo S, Karlsson A. The mitochondrial carrier SLC25A10 regulates cancer cell growth. Oncotarget 2015;6:9271–83.
40. de Sa Junior PL, Camara DAD, Porcacchia AS, Fonseca PMM, Jorge SD, Araldi RP, et al. The roles of ROS in cancer heterogeneity and therapy. Oxid Med Cell Longev 2017;2017:2467940.
41. He PJ, Ge RF, Mao WJ, Chung PS, Ahn JC, Wu HT. Oxidative stress induced by carboplatin promotes apoptosis and inhibits migration of HN-3 cells. Oncol Lett 2018;16:7131–8.
42. Xiang Y, Stine ZE, Xia J, Lu Y, O'Connor RS, Altman BJ, et al. Targeted inhibition of tumor-specific glutaminase diminishes cell-autonomous tumorigenesis. J Clin Invest 2015;125:2293–306.
43. Okazaki A, Gameiro PA, Christodoulou D, Laviollette L, Schneider M, Chaves F, et al. Glutaminase and poly(ADP-ribose) polymerase inhibitors suppress pyrimidine synthesis and VHL-deficient renal cancers. J Clin Invest 2017;127:1631–45.
44. Ledermann JA, Harter P, Gourley C, Friedlander M, Vergote I, Rustin G, et al. Overall survival in patients with platinum-sensitive recurrent serous ovarian cancer receiving olaparib maintenance monotherapy: an updated analysis from a randomised, placebo-controlled, double-blind, phase 2 trial. Lancet Oncol 2016; 17:1579–89.
45. Noordermeer SM, van Attikum H. PARP inhibitor resistance: a tug-of-war in BRCA-mutated cells. Trends Cell Biol 2019;29:820–34.
46. Park Y, Chui MH, Suryo Rahmanto Y, Yu ZC, Shamanna RA, Bellani MA, et al. Loss of ARID1A in tumor cells renders selective vulnerability to combined ionizing radiation and PARP inhibitor therapy. Clin Cancer Res 2019;25:5584–94.